ACS NANO

Cite This: ACS Nano 2018, 12, 5130–5140

www.acsnano.org

ARTICLE

Direct Laser Writing of Nanophotonic Structures on Contact Lenses

Bader AlQattan,*,† Ali K. Yetisen,‡ and Haider Butt*,†

†Nanotechnology Laboratory, School of Engineering, and ‡School of Chemical Engineering, University of Birmingham, Birmingham B15 2TT, United Kingdom

Supporting Information

ABSTRACT: **Contact lenses are ubiquitous biomedical devices used for vision correction and cosmetic purposes. Their application as quantitative analytical devices is highly promising for point-of-care diagnostics. However, it is a challenge to integrate nanoscale features into commercial contact lenses for application in low-cost biosensors. A neodymium-doped yttrium aluminum garnet (Nd:YAG) laser (1064 nm, 3 ns pulse, 240 mJ) in holographic interference patterning mode was utilized to produce optical nanostructures over the surface of a hydrogel contact lens. One-dimensional (925 nm) and two-dimensional (925 nm × 925 nm) nanostructures were produced on contact lenses and analyzed by spectroscopy and angle-resolve measurements. The holographic properties of these nanostructures were tested in ambient moisture, fully hydrated, and artificial tear conditions. The measurements showed a rapid tuning of optical diffraction from these nanostructures from 41 to 48°. The nanostructures were patterned near the edges of the contact lens to avoid any interference and obstruction to the human vision. The formation of 2D nanostructures on lenses increased the diffraction efficiency by more than 10%. The versatility of the holographic laser ablation method was demonstrated by producing four different 2D nanopattern geometries on contact lenses. Hydrophobicity of the contact lens was characterized by contact angle measurements, which increased from 59.0° at pristine condition to 62.5° at post-nanofabrication. The holographic nanostructures on the contact lens were used to sense the concentration of Na^+ ions. Artificial tear solution was used to simulate the conditions in dry eye syndrome, and nanostructures on the contact lenses were used to detect the electrolyte concentration changes ($\pm$47 mmol L^{-1}). Nanopatterns on a contact lens may be used to sense other ocular diseases in early stages at point-of-care settings.**

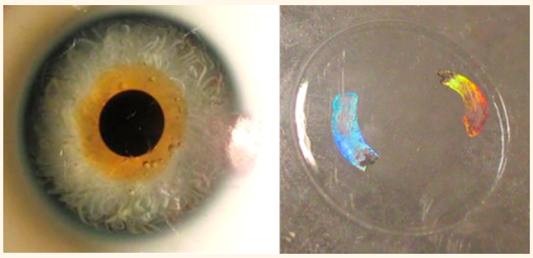

KEYWORDS: *contact lenses, holographic laser ablation, diffraction gratings, optical devices, surface wettability, sensors*

Ocular diseases are associated with increasing healthcare costs involving visual acuity tests, prescriptions of eye drops, corrective lenses, and eye surgeries. For instance, diabetic macular edema, which is the leading cause of blindness among working age adults in the United Kingdom, degrades visual acuity because of the inflammation on the central retinal thickness. This is a result of increased intraocular pressure due to damaged blood vessels in the retina, eventually causing vision impairment.[1] Graves' ophthalmopathy is another ocular condition resulting in the overproduction of thyroid hormones (hyperthyroidism), causing eyelid lag and retraction, leading to the deterioration of eye muscles and cornea.[2,3] Another major ocular disorder is glaucoma, with over 60.5 million patients globally, and it is estimated that this number will rise to 79.6 million by 2020.[4] Glucoma is caused by the increase of intraocular pressure due to the buildup of fluids, damaging the optic nerve and leading to complete blindness in worse cases.[5] Lastly, inadequate amount of tear or oil production can cause dry eye syndrome. It may be caused by Meibomian gland dysfunction (blockage of oil glands) and/or lacrimal gland dysfunction (LGD, aqueous tear deficiency). The dryness could lead to vision impairment, discomfort, and eventually blindness. Tear electrolytes such as Na^+ ion concentrations can be used to diagnose the dry eye severity at early stages.[6] Existing diagnoses of ocular vision diseases involves testing of visual acuity and prescribing corrective lenses.[7] However, there is a clear lack of quantitative point-of-care diagnostics to aid ophthalmologists. It is highly desirable to build a platform on existing commercial contact lenses to create functionalities, such as sensing biomarkers and physical changes in the eye.

Commercial silicon–hydrogel contact lenses are widely used to correct common vision problems. They are made from a variety of hydrogel compounds with different compositions, but all of them have high water content to interact with the tear film.[8] Tears have substantial diagnostic information regarding ocular diseases, and they can be used as a surrogate medium for analyzing blood chemistry.[6,10] Recently, an optical fiber sensor

Received: January 9, 2018
Accepted: April 20, 2018
Published: April 24, 2018

DOI: 10.1021/acsnano.8b00222
ACS Nano 2018, 12, 5130–5140

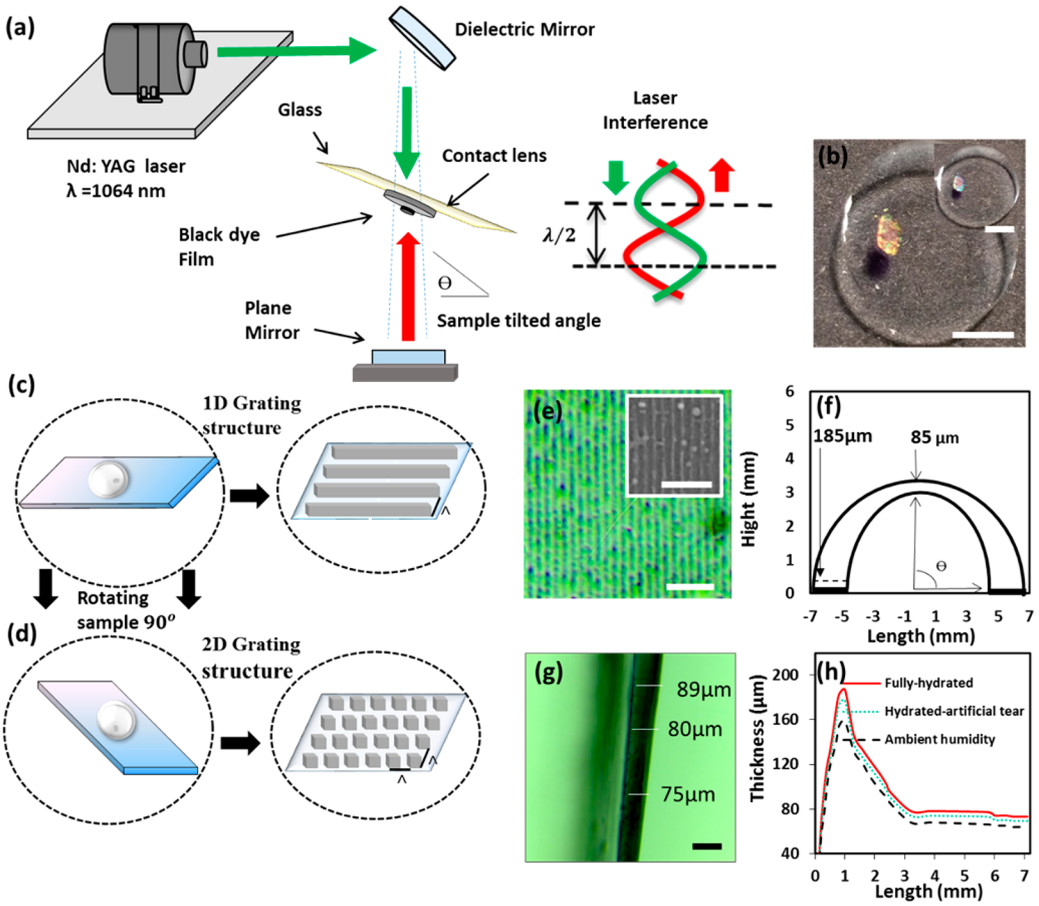

Figure 1. Fabrication of 1D nanopatterns on a contact lens through DLIP in holographic Denisyuk reflection mode. (a) Nd:YAG laser beam (1064 nm, 3.5 ns) was guided by a mirror and passed through a dyed contact lens and reflected back from a plane mirror to ablate localized regions in the recording medium. (b) Fabricated ink-based holographic nanostructures on contact lenses (scale bar = 5 mm). Schematics of (c) 1D and (d) 2D nanostructures. (e) Optical microscopy image of a 1D nanostructure surface. The inset shows the SEM image of the surface topography (scale bar = 5 μm). (f) Contact lens geometry and thickness distribution. (g) Optical image of a contact lens cross section in ambient humidity conditions (scale bar = 100 μm). (h) Contact lens thickness variations in ambient humidity, fully hydrated condition (in DI water), and hydrated condition (in artificial tear).

attached on a contact lens was developed for the quantification of tear electrolytes.[11] Various nanostructures have been fabricated within hydrogels that act as optical transducers.[9] However, integrating nanoscale features into hydrogel structures represents a fundamental challenge for producing functional contact lenses. Nanofabrication approaches to form optical structures in polymers are costly and time-consuming.[12,13] Nanostructures can be fabricated on contact lenses by contact printing,[14,15] nanoimprinting, microtransfer molding,[16] pattern replication induced by an ion field, and ultrashort laser pulse lithography. However, these fabrication approaches require multiple steps, high-energy supplies, long fabrication times, complex setups, and specialized equipment.[12,13,17] In addition, they are not capable of producing accurate and reproducible nanostructures on soft polymers.[18,19] On the other hand, most laser interference systems can produce nanostructures directly on a variety of soft and hard materials. However, multiple laser beam exposures can cause damage to soft materials, such as hydrogel-based contact lenses.[20]

Here, a holographic laser ablation method was developed to produce optical nanostructures on commercial contact lenses. A black dye was used on the contact lens to facilitate the interaction between the interfering laser beams and the lens material. The dye thickness on the contact lens was estimated through light transmission studies (Supporting Information Figure S1).[21] Low-cost optical nanostructures were rapidly created by direct laser interference patterning (DLIP) in holographic Denisyuk reflection mode to create ablative interference fringes on the contact lens surfaces.[18,21,22] One-dimensional (1D) nanostructures were fabricated on the contact lenses, and angle-resolved spectral measurements were performed to characterize their optical properties. In addition, two-dimensional (2D) nanostructures were fabricated to study the light diffraction effects with monochromatic light and broadband white light. The surface wettabilities of 2D nanostructures were determined through contact angle analysis. Hydrophilic properties may aid in increasing the tear distribution capability over the contact lens surfaces.[23] The hydrophobicity was measured by sessile drop technique as this method was fast and efficient to perform at static and dynamic angles.[24]

RESULTS AND DISCUSSION

Holographic Fabrication of Nanostructures on Contact Lenses. Figure 1a shows a schematic of the hologram recording setup in Denisyuk ablation mode. The laser beam (λ = 1064 nm) initially directed by a mirror traveled to the black dye (recording medium) deposited on the contact lens and

DOI: 10.1021/acsnano.8b00222
ACS Nano 2018, 12, 5130−5140

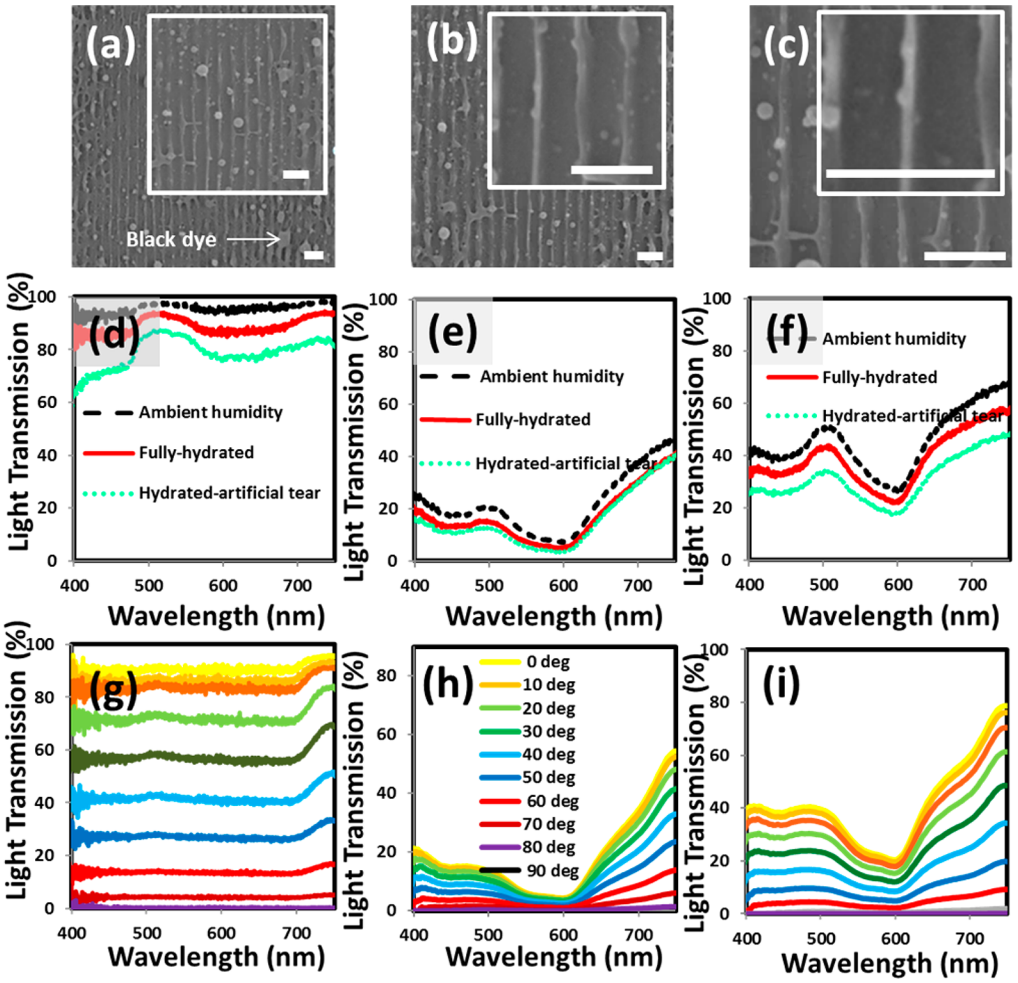

Figure 2. Electron microscopy and spectroscopy analyses of the nanopatterned contact lenses. (a−c) SEM images of 1D nanostructures on the contact lens with increasing magnification (scale bar = 5 μm). Scale bar for (c) is 2 μm. The optical transmission spectra for commercial contact lens in three states: (d) plain lens, (e) black dye coated lens, (f) and nanopatterned lens at different moisture conditions. Effect of incident light polarization on transmission in (g) fully hydrated plain lens, (h) dyed lens in ambient humidity, and (i) nanopatterned lens in ambient humidity.

reflected off from a plane mirror, placed below, to ablate the localized regions on the medium. The synthetic black dye on the contact lens surface was selectively ablated to form a holographic nanograting structure. This dye was chosen as it was able to increase the laser absorption to facilitate the ablation process.[30,31] The nanograting ablated on the contact lenses displayed diffraction and hence a rainbow hologram effect (Figure 1b). The nanopatterns were formed near the edge of the lens to prevent obstructing the vision through the center of the lens. The 1D and 2D nanostructures (through multiple exposures) were fabricated on the contact lenses (Figure 1c,d). The nanostructures fabricated were imaged through optical and scanning electron microscopy (SEM) techniques (Figure 1e).

The contact lenses have different thicknesses and concave geometry for achieving comfort on the eye (Figure 1f). A dry contact lens was sliced to measure the lens thickness variation (Figure 1g). The lens was sandwiched between glass slides for testing purposes. The plain (unmodified) thickness was measured when the lens was at ambient moisture. The thickest of the lens was ∼170 μm, which decreased to 65 μm in the central regions. On the other hand, the thickness of the lens increased to 185 μm at the edges and 85 μm in the center when it was fully hydrated with DI water (Figure 1h). The artificial tear solution decreased the thickness of the contact lens by ∼10 vol % as compared to that in DI water. This could be attributed to the decrease in Donnan osmotic pressure caused by the electrolytes in the artificial tear solution. The water content in the contact lenses was considered at equilibrium to analyze swelling degree, q_w (eq 1), where $m_{ambient}$ was the lens mass in ambient humidity and $m_{hydrated}$ was the lens mass in fully hydrated conditions.[8]

$$q_w = \left(\frac{m_{ambient}}{m_{hydrated}}\right) \times 100\ (\%) \tag{1}$$

Holographic DLIP ablates synthetic black dyes on the contact lens to form a grating. Nanoscale grooves were produced on the contact lens surface due to the high energy of laser interference (SEM in Figure 1d). The main laser ablation process on the lens was created by the laser interference of two beams: Y_I the incident laser wave (reference) and Y_R the reflected laser wave (object) from a plane mirror. The higher power is produced when two laser beams interact with each other, which can be described as

DOI: 10.1021/acsnano.8b00222
ACS Nano 2018, 12, 5130−5140

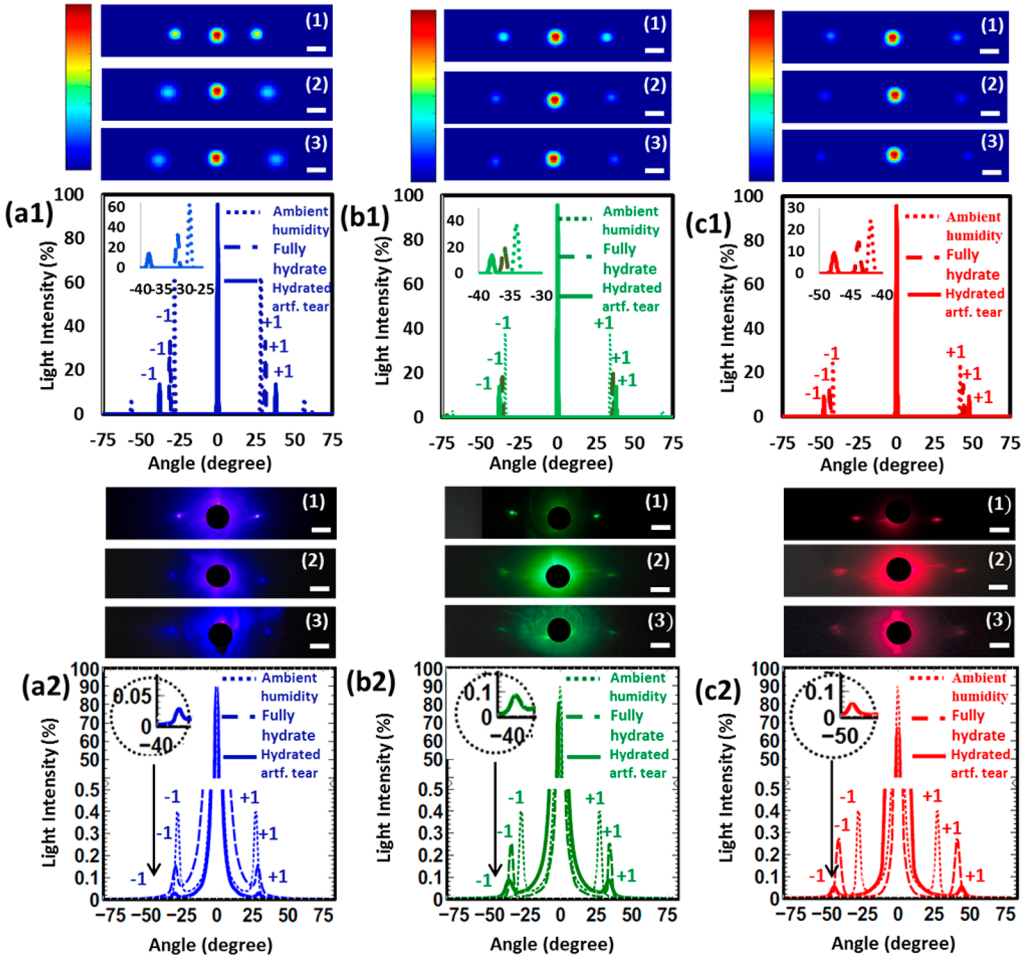

Figure 3. Simulation and experimental diffraction results for gratings with a periodicity of Λ = 925 nm on the contact lens surfaces in ambient humidity, fully hydrated, and artificial tear conditions. (a1) Simulated and (a2) experimental diffraction results for 450 nm wavelength at different humidity conditions. (b1) Simulated and (b2) experimental diffraction changes at 532 nm. (c1) Simulated and (c2) experimental diffraction for 635 nm. Scale bar = 5 cm.

$$Y_I = A \cos 2\pi\left(vt + \frac{x}{\lambda}\right) \tag{2}$$

$$Y_R = A \cos 2\pi\left(vt - \frac{x}{\lambda}\right) \tag{3}$$

$$Y = Y_I + Y_R = \left|2A \cos 2\pi\frac{x}{y}\right| \cos 2vt \tag{4}$$

where A, v, t, and λ represent the axis plane, velocity, time, and wavelength, respectively. The grating spacing depends on the exposure angle (θ) of the contact lens at ambient conditions.[22,32] At an exposure angle of 35° (from the horizontal plane), a grating spacing of 925 nm was produced. This spacing can be theoretically calculated by using the grating equation:

$$\Lambda = \frac{\lambda}{2 \sin(\theta)} \tag{5}$$

where θ is the tilt angle of the sample with the horizontal and Λ is the grating spacing. The difference between the experimental results of grating spacing and the analytical simulations was ~3% (eq 5). Figure 2a–c shows the SEM images of the fabricated nanostructures on the contact lenses and their optical transmission analyses in the wavelength range of 400–850 nm. The transmission studies were performed on plain contact lenses, lenses with thin black dye film, and the lenses with nanopatterned gratings. The lenses were tested in three phases: ambient humidity, fully hydrated with DI water, and fully hydrated with artificial tear solution. The transmission spectra for lenses changed in different humidity phases (Figure 2d). When the contact lens was in ambient humid conditions, it had the highest transmission (~95%). However, the transmission decreased in fully hydrated DI water and artificial tear conditions. The contact lens was a transparent material in ambient humidity condition, but when in wet conditions, an additional medium was absorbed by the lens' matrix. This additional media changed the effective lens thickness and the refractive index, which altered the absorption and transmission through the lens based on the refractive index of the solution (Figure 2d).

However, the deposition of the black dye on the lens highly decreased the optical transmission by around 80% (Figure 2e).[21] Increasing optical absorption contributes toward improved ablation efficiency with the Nd:YAG laser beam. However, if the absorption threshold reached >90%, the laser beam could not ablate the sample, as a low-energy laser beam passes through the sample and the returning beam from the plane mirror becomes ineffective in producing interference. The

DOI: 10.1021/acsnano.8b00222
ACS Nano 2018, 12, 5130–5140

formation of the grating on the contact lens increased the transmission efficiency by 35% (Figure 2f). Optical polarization spectroscopy was also conducted on the plain contact lens, dyed lens, and nanograting lens. Cross-polarized arrangement was used, and the polarization of incident light was varied from 0 to 90° (Figure 2g–i). Neither the fully hydrated mode, the black dye on the lens, nor the grating nanostructures seems to affect the polarization properties of incident light.

Optical Characterization of Nanogratings on Contact Lenses. Geometrical theory for diffraction was used to simulate three monochromatic light beams and their propagation through the nanogratings. The optical diffraction produced by a 1D grating with 925 nm period and 800 nm depth was modeled (details of the simulation method are in ref 17) and compared to its experimental results. The simulation was performed for lens indexes measured at ambient humidity (1.50), fully hydrated state (1.40), and hydrated with artificial tear state (1.33). Figure 3a1–c1 shows the simulated diffraction from the 1D nanostructures on the contact lens. The matching experiments were performed using three monochromatic light sources (450, 532, and 635 nm), as shown in Figure 3a2–c2.

In response to a blue laser beam illumination (450 nm), the lens nanopatterns resulted in a linear diffraction, with the first order at an angle of ∼27° (eq 6). The diffraction angles matched the theoretical diffraction equation:

$$\Lambda = \frac{\lambda m}{\sin(\theta)} \tag{6}$$

where m represents the diffraction order. When the contact lens was soaked in DI water for 20 min, the thickness of the lens increased, elevating the first-order diffraction to 29°. Then the contact lens was brought back to ambient humidity and immersed in artificial tear solution for 30 min. It was soaked for a longer time because the artificial tear had a viscosity (6.4 mm^2 s^{-1}) higher than that of water at 24° (laboratory temperature).[33] The optical analysis showed a slight increase in the first-order diffraction spot (Figure 3a2). The simulated diffraction values for the lens at ambient conditions were identical to those of the fully hydrated lens. In response to a green laser (532 nm), the lens nanopattern showed an increase in diffraction angle for the first order, at around 34° for ambient humidity conditions. The diffraction increased by 2° when the lens was fully hydrated and an additional 2° when it was hydrated with artificial tears (Figure 3b2).

A similar trend of angular change was obtained with the red laser beam illumination (635 nm), but the diffraction angle was higher than that for blue and green lasers. There was an increment of 4° between ambient moisture and fully hydrated conditions (Figure 3c2). The theoretical values were estimated based on the effective refractive index of DI water with contact lens (∼1.40) and artificial tears (1.336). Although the refractive index of pure DI water is 1.33, when it is measured within the contact lens, it becomes ∼1.40. The observations showed that the experimental results matched with the theoretical values. In the case of the artificial tears, the refractive index was equivalent to that with the human tear.[26,29,33,34] Table 1 shows the experimental and theoretical diffraction values for all the wavelengths.

The diffraction angles were influenced by the laser wavelength. Longer wavelengths of laser light diffracted through a larger angle than the shorter wavelengths. In addition, the lens in ambient moisture had the lowest diffraction angle as compared to the other two states because the lens was the thinnest in this condition. Increasing the lens thickness contributed to reducing the lens grating gap, which increased the diffraction angles. In addition, lenses soaked in artificial tear solution showed a diffraction angle higher than that of the fully hydrated lens in DI water, even though it had proportionally smaller effective thickness. This phenomenon can be attributed to the decrease in Donnan osmotic pressure within the contact lens caused by the presence of electrolytes in artificial tears. Therefore, the grating structure in the lens could be used as a generic sensor to measure analyte concentrations based on ionic changes from human eye tears *via* rapid light diffraction changes.

Table 1. Diffraction from Contact Lens Gratings Using Three Laser Beams (450, 532, and 635 nm) and Comparison to the Theoretical Values[a]

laser wavelength (nm)	Exp, amb.hum (deg)	Theo, amb-hum (deg)	Exp, full-hyd (deg)	Theo, full-hyd (deg)	Exp, hyd-tear (deg)	Theo, hyd-tear (deg)
450	27	29	29	32	31	33
532	34	35	36	37	38	39
635	41	43	45	45	48	47

[a]Exp, experimental diffraction angle; Theo, theoretical diffraction angle values; amb-hum, ambient humidity; full-hyd, fully hydrated; hyd-tear, hydrated with artificial tear solution.

The 2D periodic square nanostructures were also fabricated with holographic DLIP by multiple laser exposure. The sample was rotated 90° after the first exposure to produce the 2D square patterning, with the same tilt angle used in both exposures (Figure 1a). The 2D grating structure had a periodicity of 925 nm × 925 nm (Figure 4a). The 2D nanopatterning enhanced the transmission by 10% in all humidity conditions as compared to that of the 1D nanostructures (Figure 4b). This was due to reduced dye-coated regions and overall more transparent lenses. The diffraction measurements were performed with illuminations from three laser beams on the 2D grating structure to measure the optical properties of the lenses. The 450 nm illumination produced four diffraction spots from the 2D patterning. The diffraction points were at 27° on the x and y-axes (Figure 4c,d). Similarly, the diffraction angles were 34° for 532 nm (Figure 4e,f) and 41° for the 635 nm laser wavelengths (Figure 4g,h).

The 2D pattern was compared with 1D grating based on the diffraction efficiency (eq 2). The diffraction efficiencies ($I_{eff} = I_1/I_0$) of the nanopatterns were measured by recording the intensities of the first-order I_1 and the zero-order I_0. Although the diffraction efficiencies in the three laser illuminations were close for both 1D and 2D nanopatterns, the efficiency of the 2D grating was higher. The zero-order diffraction of the 2D grating was lower than that of the 1D grating, which indicated a higher efficiency.

To evaluate the response of the nanopatterns to broadband white light, a goniometer setup was used to carry out angle-resolved diffraction efficiency measurements. Diffraction spots from the nanostructures of contact lens were analyzed in transmission mode. The spectroscopic analysis of the rainbow diffraction was performed on a motorized rotating stage with a broadband halogen light source illumination. The rainbow distribution of grating diffraction was recorded by moving the motorized stage with 0.5° step increments from −90 to +90° (Figure 5a). The 1D and 2D rainbow diffractions of the two contact lenses were measured. The length measurements were

DOI: 10.1021/acsnano.8b00222
ACS Nano 2018, 12, 5130–5140

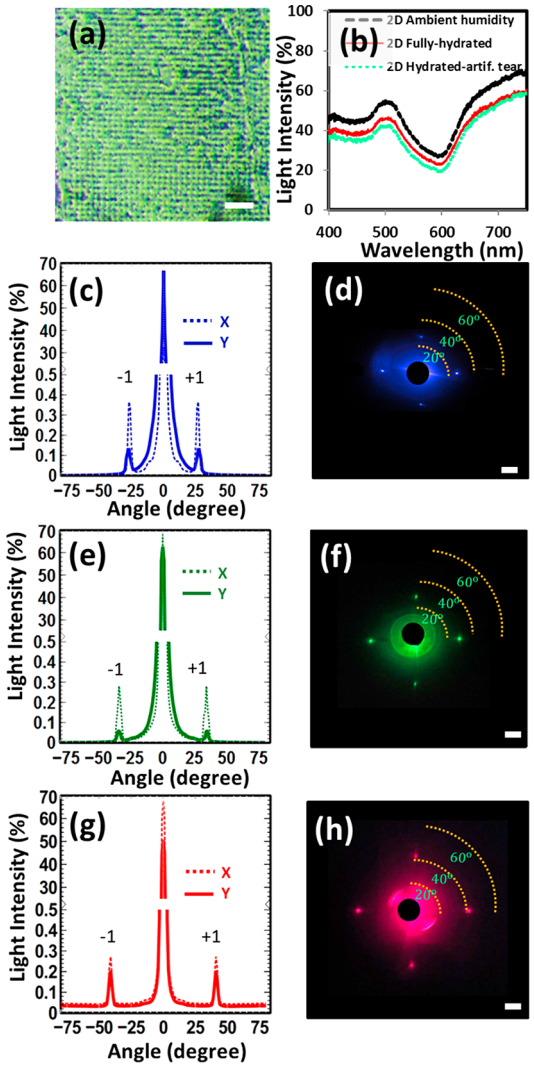

Figure 4. Optical characterization of 2D surface grating nanostructures (925 nm × 925 nm) fabricated by holographic DLIP on the contact lens. (a) Optical microscopy image of the 2D grating. (b) Transmission spectra measurements. Angle-resolved measurements of diffraction readouts in transmission mode upon illumination with three monochromatic beams: (c,d) 450 nm, (e,f) 532 nm, and (g,h) 635 nm. Scale bar = 5 cm.

based on placing a screen 16 cm away from the diffraction samples. The angle-resolved diffraction from the two lens gratings was measured at a maximum broadband light intensity to quantify the highest value of diffracted wavelength distribution. The maximization enabled the same bandwidth of grating diffraction within the range of 400−850 nm to compare the *x*-axes of 1D and 2D nanostructured patterns. The rainbow diffraction patterns of 1D and 2D lens gratings had same arcs (37−58°). These patterns showed low visible wavelength intensity at 570 nm. The diffraction efficiency of the nanopatterns at ambient humidity condition was less than 10% (Figure 5b). The 2D nanostructures formed four rainbow diffraction patterns based on the shape of the nanostructure. The *x*-axis of the 2D grating generated a trend and intensity similar to that of the 1D rainbow diffraction patterns. The second rainbow diffraction of the 2D grating on the *y*-axis had lower intensity. Figure 5c shows a holographic contact lens attached to an artificial eye model, showing the location of the nanostructure. The 2D rainbow image displayed diffraction on the *x*- and *y*-axes (Figure 5d).

Fabricating nanostructures on the contact lens can change the surface contact angle as well as the optical properties. If the contact angle increases due to the nanopatterning of the surface, then the contact lens will become more hydrophobic. Therefore, its softness will decrease and its suitability for human eye wear will become a challenge as it can cause irritation.[35] The hydrophobicity of unmodified contact lens with sessile drop test (5 μL) was ∼59°,[36] whereas the 1D nanopatterned contact angle displayed 62.8° (Figure 1d). Four different nanopatterning structures were produced for this experiment. The 1.28 μm × 1.28 μm structure showed structural patterns similar to those of the earlier 2D nanostructure, but it had a relatively larger grating spacing (Figure 6a1). However, the diffraction from the pattern showed two orders on each side of the *x*- and *y*-axes, with eight diffraction spots in total (Figure 6b1). The 2D square structure produced four identical rainbow diffraction patterns but closer to the zero order (Figure 6c1). The square nanopatterning showed some increase in the contact angle, reaching ∼71° (Figure 6d1). The second nanostructure was a rectangular pattern and had a grating size of 1.68 μm × 1.45 μm (Figure 6a2). It produced 12 diffraction spots, which were influenced from the grating spacing and shape (Figure 6b2).[22] In addition, it created four visible rainbow diffraction patterns (Figure 6c2), and the contact angle was lower than that in the first nanostructure (Figure 6d).

The next nanostructure was a rectangular pattern produced by three laser pulse exposures to obtain spacings of 0.85 μm × 2.4 μm (Figure 6a3). The 2D nanostructure produced three horizontal sets of diffraction spots (Figure 6b3). Two orders of rainbow diffraction were produced in each axis (Figure 6c3). The contact angle showed an increase of 11° as compared to the contact lens in ambient humidity (Figure 6d3). The final structure was fabricated with three laser pulses and had a smaller nanostructure geometry between large gaps (Figure 6a4). The contact angle measured was ∼62.5°, closest to the 1D nanopatterned lens and the unmodified contact lens (Figure 6b4).

The holographic DLIP system enabled different types of nanopatterns to be produced on the soft and fragile surfaces of the lens. The contact lens material (silicon−hydrogel), which is not purely solid at ambient humidity conditions, withstood up to three laser pulses without significant damage to its relatively thin matrix. The four different nanoscale shapes fabricated had an effect on the arrangement of diffraction distributions, with grating spacing influencing the location of the diffraction spots. Structures shown in Figure 6a1,a3 displayed an increase in the contact angle, although the structure area on the lens was relatively smaller (2 mm). The nanostructure geometries can be easily optimized to tailor the wetting properties of contact lenses to suit various eye conditions and comfort levels.

The nanopatterned contact lenses were also used as generic refractive index sensors. One of the 2D nanostructure patterns (925 nm × 1555 nm) was used to sense analytes in the artificial tears. The *x*-axis diffraction pattern (responding to the 925 nm spacing) was used to detect different concentrations of Na^+ ions in tears, as an increase or decrease in electrolytes can be an indication of eye disorders.[6] The normal concentration of Na^+ and Cl^- ions in human tears is 142 and 135 mmol L^{-1}, respectively.[37] Different concentrations were prepared in DI water for testing purposes. The contact lens was placed in a

DOI: 10.1021/acsnano.8b00222
ACS Nano 2018, 12, 5130−5140

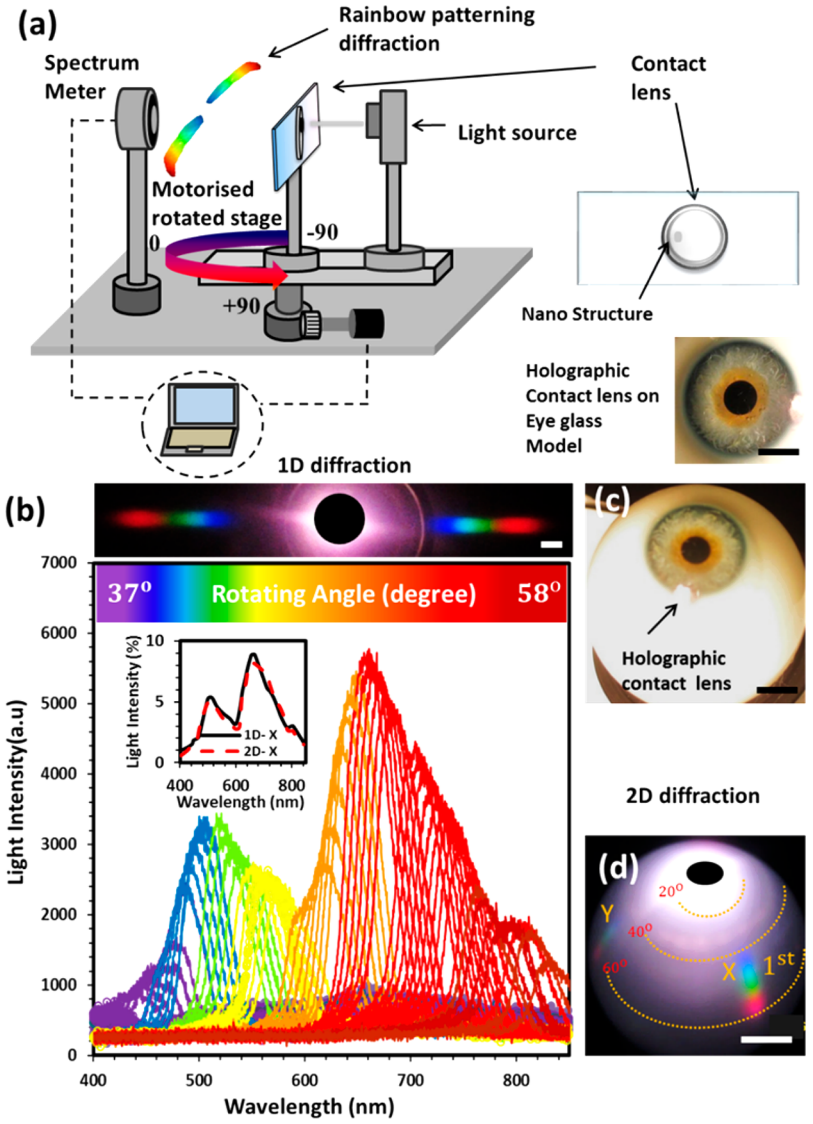

Figure 5. Angle-resolved measurements of the 1D and 2D diffraction patterns from the contact lens. (a) Spectroscopic measurement of the rainbow diffraction of the 1D nanostructure over the contact lens in transmission mode using a broadband light. Scale bar = 5 mm. (b) Broadband white light angular measurements for 1D and 2D gratings along the *x*-axis. Scale bar = 5 mm. (c) Holographic contact lens on an eye model. (d) 2D rainbow diffraction of the holographic contact lens on a spherical screen. Scale bar = 1 cm.

cuvette for continuous optical measurements. The black dye and nanostructured contact lenses were tested in transmission mode in the cuvette at different Na^+ ion concentrations. The transmission of the black ink dye on the contact lens showed no significant change for varying Na^+ ions concentrations (0–230 mmol L^{-1}) but decreased at higher concentrations (Figure 7a).

The transmission increased through the nanopatterned contact lens, and likewise, the diffraction intensity and angle changed with increasing Na^+ ions in the solution (Figure 7b). The nanogratings on the lens surface had periodic grooves, and the refractive index of the groove medium changed the gratings' diffraction properties. Hence, the variation in transmission was based on the change in the effective refractive index due to the change of electrolyte concentrations (Figure 7c and Supporting Information Table S4). The diffraction measurements for the contact lens nanostructures were carried out with a 635 nm laser illumination. The readings were recorded every 10 min with different electrolyte concentrations. This time frame was selected as a sufficient period to achieve equal comparison between all concentrations. The results showed an increase in diffraction angle with increasing concentration of Na^+ ions (Figure 7d). It is hypothesized that the increase in ion concentrations caused the lens to expel water and shrink, leading to a decrease in grating spacings and hence an increase in diffraction angles. The lenses can be further functionalized by using engineered dyes/materials which respond to specific analyses such as glucose, electrolytes, or proteins in tears.

We also fabricated various holographic patterns (nanostructures) on contact lenses to show the flexibility and uniformity of the laser-based fabrication method (Figure 7e1–h2). The holographic structures on contact lenses displayed rainbow diffraction effects upon illumination with broadband white light. These nanostructures can be designed in various shapes (rings/patches) and can be used for sensing and also to enhance the appearance of the contact lenses, for example, for cosmetic purposes. Furthermore, the nanopatterns may change their visible colors in response to changes in the curvature of the

DOI: 10.1021/acsnano.8b00222
ACS Nano 2018, 12, 5130–5140

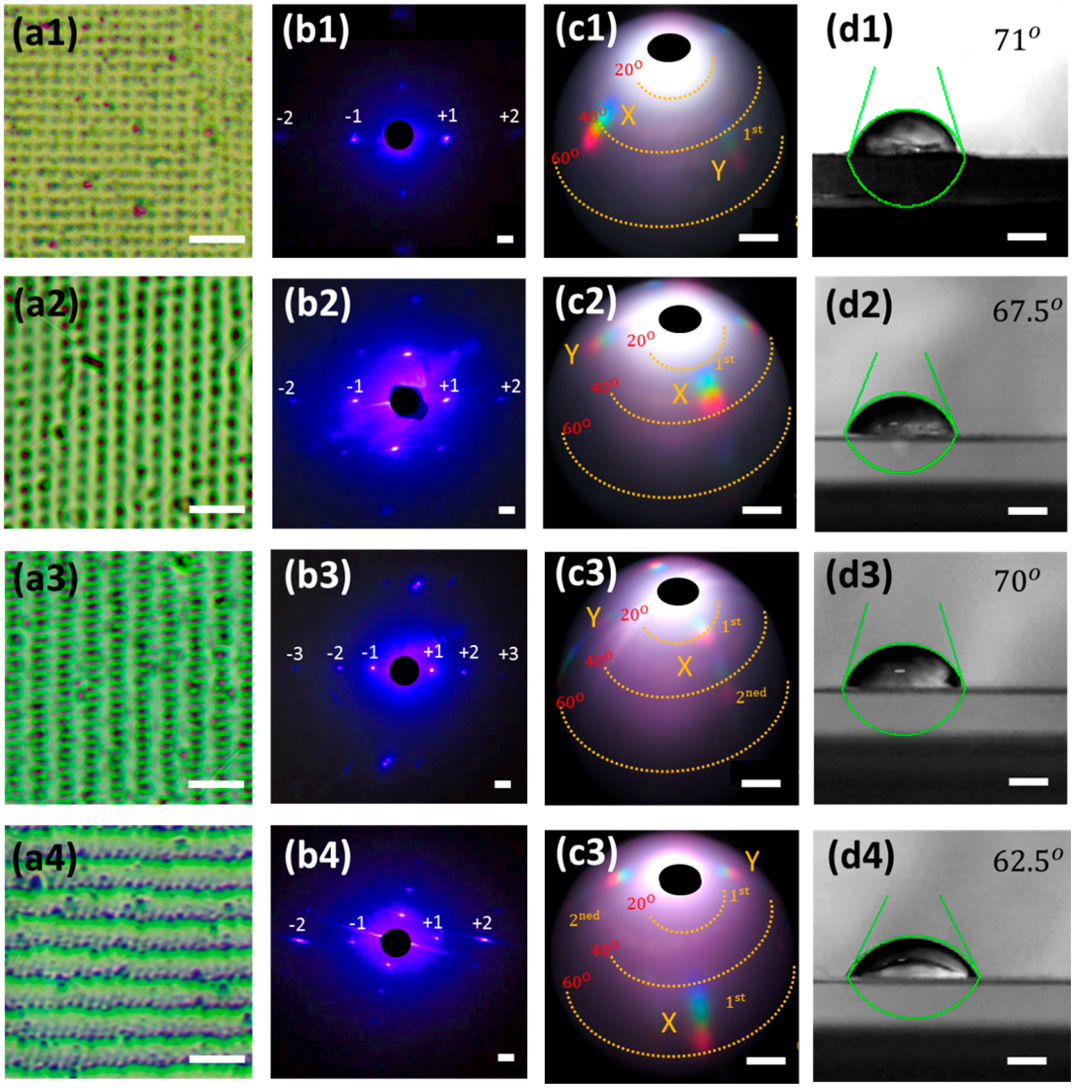

Figure 6. Optical microscopy images of 2D nanostructures with different geometries on contact lenses: (a1) 1.3 μm × 1.3 μm, (a2) 1.7 μm × 1.5 μm, (a3) 0.9 μm × 2.4 μm, and (a4) 0.9 μm × 2.7 μm. Scale bars = 5 μm. (b1−b4) Diffraction of monochromatic light (450 nm) *via* 2D patterned arrays. Scale bar = 1.0 cm. (c1−c4) Rainbow diffraction from 2D patterned arrays. Scale bar = 1.0 cm. (d1−d4) Contact angle measurements of 2D nanostructures on contact lenses. Scale bars = 1.0 μm.

eyes, hence allowing the clinicians to monitor ocular pressure in the diagnosis/monitoring of glaucoma.

With the low-cost and direct holographic DLIP method, optical nanostructures were produced on commercial contact lenses. Depositing a synthetic black dye on the contact lens allowed the formation of surface nanogratings on the hydrogel matrix using a pulsed Nd:YAG laser. The contact lenses fabricated in this work were tested over a year, showing no signal drift or hysteresis, indicating long shelf life. These optical nanostructures were fabricated at the edge of the contact lens to prevent any sight obstruction or interference of human vision. The formation of 2D nanostructures on the lens surface increased the diffraction intensity by more than 10% as compared to that of the 1D nanostructures. The versatility of holographic laser ablation method was demonstrated by creating four different 2D nanopatterns with different designs on the contact lens surface without significantly changing the hydrophilicity properties. Additionally, direct sensing of Na^+ ions was conducted by measuring the transmission and diffraction properties. Ocular conditions such as edema, Graves' eye disease, and glaucoma can be potentially monitored from the change of eye curvature, which will have a direct influence on the shape and spacing of nanostructures fabricated on the lens surface. Other ocular diseases can also be predicted in early stages when the contact lens matrix is functionalized and integrated with the nanostructures to recognize concentration changes of analytes and proteins in human tears.

MATERIALS AND METHODS

Preparation of the Recording Media on Contact Lenses. Commercial silicon−hydrogel contact lenses were used in this work (Narafilcon A, Acuvue, Johnson & Johnson). All lenses had a dioptric power of −0.5 with a base curve of 8.6 mm and a total length of 14.2 mm.[25] The oxygen permeability of the contact lenses was 100×10^{-11}. These contact lenses were fabricated by the copolymerization of monofunctional polydimethylsiloxane (MPMDSM), *N*,*N*-dimethylacrylamide (DMA), hydroxyethyl methacrylate (HEMA), siloxane macromer, tetraethylene glycol dimethacrylate (TEGDMA), and polyvinylpyrrolidone (PVP), and they can accommodate 46 vol % of water (ESI Material, Table S2).[26−29] To prepare a sample, the contact lens was dehydrated and attached to a glass slide, and a synthetic black dye (thickness ∼915 nm) was directly deposited on it. The thickness

DOI: 10.1021/acsnano.8b00222
ACS Nano 2018, 12, 5130−5140

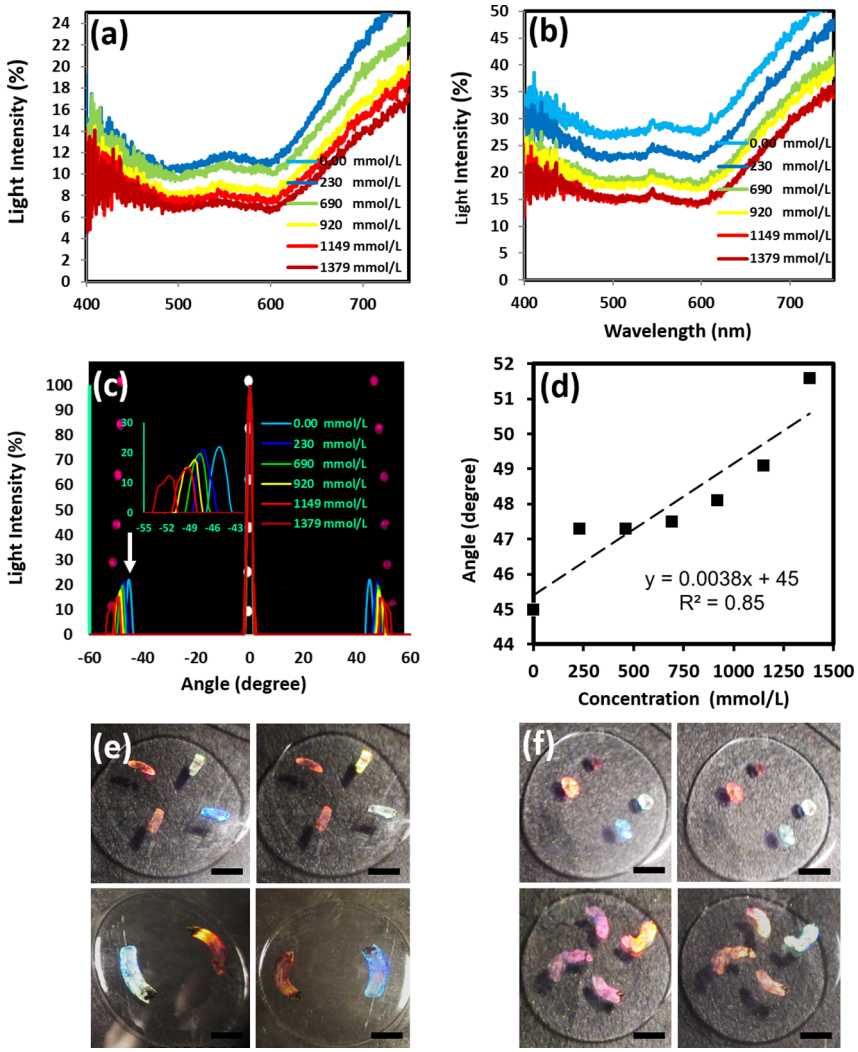

Figure 7. Light transmission spectra as a function of Na^+ ion concentrations: (a) dye-coated lens and (b) nanograting on the contact lens. (c) Diffraction measurements on the nanopatterned contact lens at different Na^+ ion concentrations. (d) Variation with diffraction angles with Na^+ ion concentrations (e−h) Different designs (rings/patches) of holographic nanostructures fabricated on contact lenses. Each image demonstrates the diffraction colors observed at various angles (scale bar = 5 mm).

of dye on the contact lens was estimated based on the transmission of different spin-coated thicknesses on glass substrates and compared with the published work. This thickness was chosen because it optimized laser interference in Denisyuk mode to provide a well-defined nanostructure to interact with the laser beam (Supporting Information Figure S1).[21] The lens was hydrated with deionized (DI) water and artificial tear solution (Hypromellose 0.3 wt % eye drop).[27,28] In addition, the contact lens was tested in a cuvette for continuous sensing measurements.

Fabrication of Diffraction Gratings on Contact Lenses. Holographic direct laser interference patterning was used in Denisyuk reflection mode. A nanosecond pulsed laser (λ = 1064 nm, 240 mJ, 3.5 ns) was used to ablate the black dye deposited over the contact lens surface. The interference between the incident and reflected laser beams ablated localized regions of the dye medium. The exposure angle of all dye films was 35° from the surface plane of the plane mirror, which was used to produce the object beam in the holography setup.

Spectroscopic Measurements of the Ink Gratings. The diffraction of light from 1D gratings was analyzed by normally illuminating the periodic samples with blue (λ = 450 nm), green (λ = 532 nm), and red (λ = 635 nm) laser beams and recording the transmitted light on a flat screen placed perpendicularly 17 cm away from the sample. The testing was performed on plain lenses, black dyed lenses, and on lenses with patterned nanogratings, in three phase conditions (dry lens, wet with DI water, and wet with artificial tear solution).

Angle-Resolved Measurements of the Gratings. A halogen light source (HL-2000, Ocean Optics) and a goniometer setup were used to carry out angle-resolved measurements of diffraction efficiency on the ink nanogratings. The sample was placed 17 cm away from the optical probe to analyze the diffracted wavelengths. A motorized rotating stage was used for the broadband spectroscopic analysis of the rainbow diffraction produced by the nanostructure gratings. The rotation stage had a precision of 0.5° step from −90 to +90°.

ASSOCIATED CONTENT

Supporting Information

The Supporting Information is available free of charge on the ACS Publications website at DOI: 10.1021/acsnano.8b00222.

Preparation of the lenses; black ink gratings at different thicknesses in transmission and diffraction modes; material properties of the contact lenses; NaCl in DI water at different concentrations and ellipsometry equivalent reading of refractive index values (PDF)

DOI: 10.1021/acsnano.8b00222
ACS Nano 2018, 12, 5130−5140

AUTHOR INFORMATION

Corresponding Authors

*E-mail: bxa301@bham.ac.uk.
*E-mail: h.butt@bham.ac.uk.

ORCID

Ali K. Yetisen: 0000-0003-0896-267X
Haider Butt: 0000-0003-2434-9525

Notes

The authors declare no competing financial interest.

ACKNOWLEDGMENTS

The authors thank the Wellcome Trust for research funding.

REFERENCES

(1) Do, D. V.; Nguyen, Q. D.; Boyer, D.; Schmidt-Erfurth, U.; Brown, D. M.; Vitti, R.; Berliner, A. J.; Gao, B.; Zeitz, O.; Ruckert, R.; Schmelter, T.; Sandbrink, R.; Heier, J. S. One-Year Outcomes of the da Vinci Study of VEGF Trap-Eye in Eyes with Diabetic Macular Edema. *Ophthalmology* **2012**, *119*, 1658−1665.

(2) Weetman, A. P. *N. Engl. J. Med.* **2000**, *343*, 1236−1248.

(3) Boelaert, K.; Torlinska, B.; Holder, R. L.; Franklyn, J. A. Subjects with Hyperthyroidism Present with a Paucity of Symptoms and signs: a large Cross-Sectional Study. *J. Clin. Endocrinol. Metab.* **2010**, *95*, 2715−2726.

(4) Quigley, H. A.; Broman, A. T. The Number of People with Glaucoma Worldwide in 2010 and 2020. *Br. J. Ophthalmol.* **2006**, *90*, 262−267.

(5) Lee, S. J.; Lee, C. K.; Kim, W. S. Long-Term Therapeutic Efficacy of Phacoemulsification with Intraocular Lens Implantation in Patients with Phacomorphic Glaucoma. *J. Cataract Refractive Surg.* **2010**, *36*, 783−789.

(6) Yetisen, A. K.; Jiang, N.; Ruiz-Esparza, G. U.; Zhang, Y. S.; Tamayol, A.; Medina-Pando, S.; Gupta, A.; Wolffsohn, J. S.; Butt, H.; Khademhosseini, A.; Yun, S. H. Paper-Based Based MicrofluidicSystem for Tear Electrolyte Analysis. *Lab Chip* **2017**, *17*, 1137−1148.

(7) Ouellette, A. L.; Li, J. J.; Cooper, D. E.; Ricco, A. J.; Kovacs, G. T. Evolving Point-of-Care Diagnostics Using Up-Converting Phosphor Bioanalytical Systems. *Anal. Chem.* **2009**, *81*, 3216−3221.

(8) Guryca, V.; Hobzová, R.; Prádný, M.; Sirc, J.; Michálek, J. Surface Morphology of Contact Lenses Probed with Microscopy Techniques. *Cont Lens Anterior Eye* **2007**, *30*, 215−222.

(9) Yetisen, A. K.; Butt, H.; Volpatti, L. R.; Pavlichenko, I.; Humar, M.; Kwok, S. J.; Koo, H.; Kim, K. S.; Naydenova, I.; Khademhosseini, A.; Hahn, S. K.; Yun, S. H. Photonic Hydrogel Sensors. *Biotechnol. Adv.* **2016**, *34*, 250−271.

(10) Khuri, R. N. Device for Determination of Tear Constituents. U.S. Patent Appl. US5352411A, 1994.

(11) Harvey, D.; Hayes, N. W.; Tighe, B. Fibre Optics Sensors in Tear Electrolyte Analysis: Towards a Novel Point of Care potassium Sensor. *Cont Lens Anterior Eye* **2012**, *35*, 137−144.

(12) Alqurashi, T.; Penchev, P.; Yetisen, A. K.; Sabouri, A.; Ameen, R. M.; Dimov, S.; Butt, H. Dimov S.; Butt, H. Femtosecond Laser Directed Fabrication of Optical Diffusers. *RSC Adv.* **2017**, *7*, 18019−18023.

(13) Sabouri, A.; Anthony, C. J.; Prewett, P. D.; Bowen, J.; Butt, H. Effects of Current on Early stages of Focused Iion Beam Nano-Machining. *Mater. Res. Express* **2015**, *2*, 055005.

(14) Jiao, L.; Fan, B.; Xian, X.; Wu, Z.; Zhang, J.; Liu, Z. Creation of Nanostructures with Poly (Methyl Methacrylate)-Mediated Nano-transfer Printing. *J. Am. Chem. Soc.* **2008**, *130*, 12612−12613.

(15) Kumar, A.; Whitesides, G. M. Features of Gold Having Micrometer to Centimeter Dimensions can be Formed Through a Combination of Atamping with an Elastomeric Stamp and Sn Slkanethiol "Ink"Followed by Chemical Etching. *Appl. Phys. Lett.* **1993**, *63*, 2002−2004.

(16) Cavallini, M.; Murgia, M.; Biscarini, F. Patterning a Conjugated Molecular Thin Film at Submicron Scale by Modified Microtransfer Molding. *Nano Lett.* **2001**, *1*, 193−195.

(17) Alqurashi, T.; Montelongo, Y.; Penchev, P.; Yetisen, A. K.; Dimov, S.; Butt, H. Femtosecond Laser Ablation of Transparent Microphotonic Devices and Computer-Generated Holograms. *Nanoscale* **2017**, *9*, 13808−13819.

(18) Zhao, Q.; Yetisen, A. K.; Sabouri, A.; Yun, S. H.; Butt, H. Printable Nanophotonic Devices *via* Holographic Laser Ablation. *ACS Nano* **2015**, *9*, 9062−9069.

(19) Khalid, M. W.; Ahmed, R.; Yetisen, A. K.; AlQattan, B.; Butt, H. Holographic Writing of Ink-Based Phase Conjugate Nanostructures *via* Laser Ablation. *Sci. Rep.* **2017**, *7*, 10603.

(20) Müller-Meskamp, L.; Schubert, S.; Roch, T.; Eckhardt, S.; Lasagni, A. F.; Leo, K. Transparent Conductive Metal Thin-Film Electrodes Structured by Direct Laser Interference Patterning. *Adv. Eng. Mater.* **2015**, *17*, 1215−1219.

(21) AlQattan, B.; Benton, D.; Yetisen, A. K.; Butt, H. Laser Nanopatterning of Colored Ink Thin Films for Photonic Devices. *ACS Appl. Mater. Interfaces* **2017**, *9*, 39641−39649.

(22) AlQattan, B.; Butt, H.; Sabouri, A.; Yetisen, A. K.; Ahmed, R.; Mahmoodi, N. Holographic Direct Pulsed Laser Writing of Two-Dimensional Nanostructures. *RSC Adv.* **2016**, *6*, 111269.

(23) Lin, M. C.; Svitova, T. F. Contact Lenses Wettability in Vitro: Effect of Surface-Active Ingredients. *Optom. Vis. Sci.* **2010**, *87*, 440.

(24) Uyama, Y.; Inoue, H.; Ito, K.; Kishida, A.; Ikada, Y. Comparison of Different Methods for Contact Angle Measurement. *J. Colloid Interface Sci.* **1991**, *141*, 275−279.

(25) Morgan, P. B.; Chamberlain, P.; Moody, K.; Maldonado-Codina, C. Ocular Physiology and Comfort in Neophyte Subjects Fitted with Daily Disposable Silicone Hydrogel Contact Lenses. *Cont Lens Anterior Eye* **2013**, *36*, 118−125.

(26) González-Méijome, J. M.; Lira, M.; López-Alemany, A.; Almeida, J. B.; Parafita, M. A.; Refojo, M. F. Refractive Index and Equilibrium Water Content of Conventional and Silicone Hydrogel Contact Lenses. *Ophthalmic Physiol Op.* **2006**, *26*, 57−64.

(27) Varikooty, J.; Keir, N.; Richter, D.; Jones, L. W.; Woods, C.; Fonn, D. Comfort Response of Three Silicone Hydrogel Daily Disposable Contact Lenses. *Optom. Vis. Sci.* **2013**, *90*, 945−953.

(28) Cerdeira, A. M.; Mazzotti, M.; Gander, B. Miconazole Nanosuspensions: Influence of Formulation Variables on Particle Size Reduction and Physical Stability. *Int. J. Pharm.* **2010**, *396*, 210−218.

(29) Rahman, M. Q.; Chuah, K. S.; Macdonald, E. C. A.; Trusler, J. P. M.; Ramaesh, K. The Effect of pH, Dilution, and Temperature on the Viscosity of Ocular Lubricants-shift in rheological parameters and potential clinical significance. *Eye* **2012**, *26*, 1579.

(30) Magnusson, R.; Gaylord, T. Analysis of Multiwave Diffraction of Thick Gratings. *J. Opt. Soc. Am.* **1977**, *67*, 1165−1170.

(31) Vasconcellos, F. C.; Yetisen, A. K.; Montelongo, Y.; Butt, H.; Grigore, A.; Davidson, C. A.B.; Blyth, J.; Monteiro, M. J.; Wilkinson, T. D.; Lowe, C. R. Printable Surface Holograms *via* Laser Ablation. *ACS Photonics* **2014**, *1*, 489−495.

(32) Zhao, Q.; Yetisen, A. K.; Anthony, C.; Fowler, W.; Yun, S. H.; Butt, H. Printable Ink Holograms. *Appl. Phys. Lett.* **2015**, *107*, 041115.

(33) Bilalov, E.; Avanesova, A. Evaluation of Prophylaxis of Dry Eye Syndrome Associated with Soft Contact lenses. *Med. Health Sci. J.* **2014**, *4*, 186−190.

(34) Craig, J. P.; Simmons, P. A.; Patel, S.; Tomlinson, A. Refractive index and Osmolality of Human Tears. *Optom. Vis. Sci.* **1995**, *72*, 718−724.

(35) Campbell, D.; Carnell, S. M.; Eden, R. J. Eden RJ. Applicability of Contact Angle techniques used in the analysis of contact lenses, Part I. *Eye & Contact Lens* **2013**, *39*, 254−262.

(36) Read, M. L.; Morgan, P. B.; Kelly, J. M.; Maldonado-Codina, C. Dynamic Contact Angle Analysis of Silicone Hydrogel Contact Lenses. *J. Biomater. Appl.* **2011**, *26*, 85−99.

DOI: 10.1021/acsnano.8b00222
ACS Nano 2018, 12, 5130−5140

(37) Bright, A. M.; Tighe, B. J. The Composition and Interfacial Properties of Tears, tear substitutes and tear models. *Journal of the B.C.L.A* **1993**, *16*, 57−66.

DOI: 10.1021/acsnano.8b00222
ACS Nano 2018, 12, 5130−5140